Problems and Solutions in high-rate multi-channel Hybrid Photodiode design: The CMS Experience

Priscilla B. Cushman and Adriaan H. Heering

***Abstract*- The unique conditions of the CMS experiment (4 Tesla magnetic field, restricted access, high neutron radiation, and 25 ns bunch-crossings) necessitated the development of a new type of high-rate multi-channel hybrid photodiode for the tile/fiber hadronic calorimeter. New complexities arose in the push toward high-rate operation, necessitating design changes in the diode structure and surface treatment. The product is now capable of high-rate operation with low crosstalk and leakage current. Lifetime studies of high voltage behavior, total charge, and irradiation have shown that the tubes will survive the 10 years of CMS running with only a few percent change in gain and manageable leakage current rise.**

I. Introduction

The CMS Hadronic Calorimeter [1] is a sampling calorimeter composed of scintillating tiles alternating with brass absorber arranged in a projective tower geometry pointing back to the interaction region. Energy deposited in each active scintillator element produces blue light, a few percent of which is captured and re-emitted at 520 nm in wavelength-shifting (WLS) fibers coiled inside the tiles.

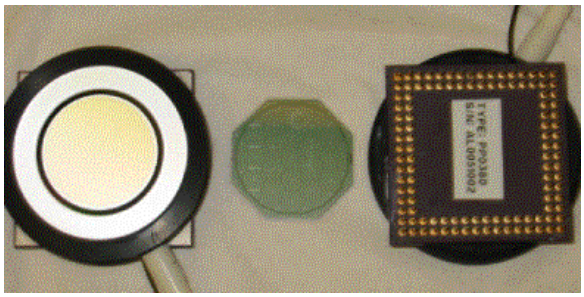

Fig. 1. The front and back of the CMS custom HPD on either side of the 19-channel hexagonal close-packed diode array which is mounted inside.

Clear fiber mated to the WLS fiber routes the light to readout boxes located outside the calorimeter, but still within the 4 Tesla solenoid field. The fibers are originally arranged by horizontal layer, but are sorted into bundles corresponding to towers within the readout box. The bundles can have as few as 2 fibers and as many as 18, depending on the number of tiles stacked into a tower. The readout solution optimized cost per channel by providing 19 and 73-channel Hybrid Photodiodes (HPD's) in identical housings and pin-out patterns, though a recent economic measure eliminated the thin compensation layer, and thus the 73-channel (2-3 fibers/bundle) version entirely.

II. Custom Tube Design

A development project was initiated with DEP[1] to produce a tube which met the CMS criteria after beam tests at CERN showed HPD's to be superior to APD's for this application. [2],[3]. Fig. 1 shows photographs of the final tube and internal diode array. The following changes to the commercially available 7-channel tube design were necessary.

1) *Reduction in the accelerating gap*

The gap was reduced from 5.3 mm to 3.3 mm to minimize image shift due to E x B effects. This relaxed tolerances on alignment of the tubes parallel to the B-field to 2°, such that optical crosstalk due to image shift was eliminated, as long as 400 ìm was maintained between the edges of fiber bundles. Smaller accelerating gaps were rejected as posing too high a risk of high voltage breakdown, since a gain of 2500 requires a 12 kV operating voltage over 10 years of CMS running.

2) *Larger surface area*

The area was enlarged in order to accommodate the larger fiber bundles along with an additional 400 µm of space between bundles. This additional space is needed not only to prevent optical crosstalk between pixels in the event of a non-parallel alignment of tube axis with magnetic field, but also in order to maintain the mechanical integrity of the plastic disk which presents the fiber bundles to the face of the tube. The 487 mm² active area is realized by increasing the diameter of a nominal 25 mm format tube to 27 mm, putting the perimeter of the active area closer to the walls of the tube than had ever been attempted before, raising concerns about charging of the body walls. Space charge effects were not a problem; instead, the tight space made

Manuscript received November 8, 2001. This work was supported in part by the U.S. Department of Energy under Grant DOE/DE-FG02-94ER40823

P.B.Cushman is with the Physics Department at the University of Minnesota, Minneapolis, MN, USA (phone: 612-626-8917, e-mail: prisca@physics.umn,edu)

A.H.Heering is with the Physics Dept., University of Minnesota, Minneapolis, MN, USA (telephone: 612-626-1015, e-mail: arjan@physics.umn,edu)

[1] B.V. Delft Electronische Producten, Roden, Netherlands

potting difficult and was responsible for high voltage breakdown in a subset of tubes.

3) New HV feedthru designs to improve reliability.

Interior sparking to photocathode can cause sudden death as well as slow deterioration in photocathode response as pinholes are created in the fiber optic faceplate. New current spike monitoring stations were developed to detect the onset of sparking before deterioration. They also helped identify the problem, which was eliminated by new potting techniques and increasing the insulation between the interior ground and photocathode. The cable sheath is also now embedded in the tube potting and extends out over the exterior cable in order to provide mechanical support.

4) Smaller, denser packing of the pixels.

Optimization of channel cost for the HCAL tower geometry, moderated by the magnetic field tolerances discussed above, led to a close-packed hexagonal array of 5.4 mm flat-to-flat pixels for towers with large bundles (19-channel version) and 2.68 mm pixels for small bundles (73-channel version). These arrays map to each other in such a way that the same vacuum feedthru design can be used for both, thus reducing the design cost of this component.

5) New ceramic vacuum feedthru design

The 73-channel device required denser pixel arrangements than ever before achieved by DEP. Work sponsored by the SSC project showed that Litton could produce multi-channel hybrid avalanche photodiodes [4] with dense pixel structure by indium bump-bonding to gold pads on a ceramic feedthru. DEP's first tubes were wire-bonded. During the high heat of photocathode processing, several pixels would frequently lose their contact or diffusion of the thin aluminum contact layer into the silicon would cause locally high leakage currents. A failed attempt by DEP to produce their own glass feedthru convinced them to follow Litton's lead. They sub-contracted with Kyocera[2] to design the multi-layer ceramic feedthru which transfers signals from a hexagonal array of bump-bonds to a standard 0.1" pitch pin grid array (see Fig. 1). In the assembly of the readout box, these pins fit to a standard zero insertion force (ZIF) socket with a locking lever. In order to assure the reliability of these contacts, a second design required gold-plating of the pins. A study conducted at DEP proved that the diffusion of gold into the Kovar pins during module brazing was not a problem.

6) Optimization of the photocathode

An S20 photocathode is applied to a Schott glass fiber optic window. The quantum efficiency is 11%-18% at 520 nm with a broad wavelength maximum. Care is taken to keep the red sensitivity low since this translates into increased dark counts.

III. Diode Design

The silicon diode is a T-type, reverse-illuminated PIN diode fabricated using epitaxial growth by Canberra[3]. The photoelectrons are converted to electron-hole pairs within the first few micrometers of the surface of the n+ layer. The holes drift through the bulk n-type silicon and are collected from the backside p+ implants, which define a hexagonal close-packed array of pixels. Additional p+ structure on the back defines a grounded ring plus six floating guard rings that maintain uniformity for the edge pixels and aids in maintaining a high breakdown voltage. At the edge of the diode, there is an n+ ring which supplies the bias voltage from the back of the diode to the front n+ surface through the bulk material. There are 40 microns between each pixel implant, but no dead space in the response uniformity.

The shape of the output pulse in response to a delta function input pulse, reveals much about the internal structure of the diode. The rising and falling edges are defined by the RC constant of the combined diode plus preamplifier and connections, whereas the central region is determined by the drift speed of the holes. The slope of the central region therefore mirrors the internal E-field generated within the diode as a function of x through the bulk:

$$E(x) = \frac{2V_d x}{d^2} + \frac{(V_b - V_d)}{d}$$

where d is the diode depth, V_d is the depletion voltage, and V_b is the applied bias. Integrating to get the current gives:

$$I(t) = e^{\left(\frac{2mV_d}{d^2}\right)t} Nqm(V_b - V_d)/d^2$$

where Nq is the total charge and ì is the hole mobility from dx/dt=ìE. This means that the output current pulse has a width given by the time for a hole to travel distance d:

$$\Delta(ns) = d^2 \ln\left(\frac{\sqrt{V_b + V_d}}{\sqrt{V_b - V_d}}\right) \Big/ mV_d$$

The plateau of the pulse is flat for low depletion voltages (or thick diodes) where the exponent in the current is small.

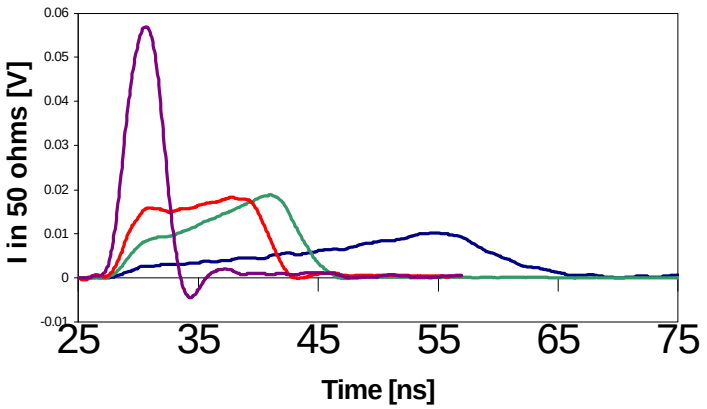

Fig. 2. Pulse shapes for (from widest to narrowest) the 300 micron and the 200 micron diodes at 80 V bias, the low-depletion, 200 micron diodes at 80 V bias and again at 500 V bias.

In Fig. 2, scope traces of the response to a 1.5 ns pulse from an LED show how the structure of the diode has changed over our development period. The conventional 300

[2] Kyocera Corporation (Fine Ceramics Division), Kyoto, Japan
[3] Canberra Semiconductor N.V., Lammerdries 25, B 2250, Olen, Belgium

µm thick, 5 kΩ-cm silicon gave wider than optimum pulses for the CMS application, so the diode thickness was reduced to 200 ìm in order to reduce d in the above equations. Despite the increased fragility of the wafers, the loss in yield has been negligible.

A further improvement can be obtained by insisting on higher ohmic silicon, which pushes down the depletion voltage. In Fig. 2, the pulse shapes from later diodes clearly show a flatter plateau and narrower width at the operating voltage of 80 V. Once the depletion voltage is small compared to the bias, the output pulse becomes square with the width $\Delta(ns) \sim d^2/\mu V_b$ and the height maintaining the total area via $h(nA) \sim Nq/\Delta$. The later diodes were also able to tolerate much higher reverse bias without breaking down, and so could be operated in a highly depleted mode: see the very narrow pulse in Fig. 2 at a bias of 500 V.

Fits using the above model to pulse width as a function of inverse applied bias shows that the low depletion diodes produce stable pulse shapes at the operating bias voltage of 80 V, whereas higher depletion voltages can be affected by variations in the delivered bias. We therefore specified a minimum resistivity of 8 kΩ-cm (V_d < 35 V). The capacitance per pixel when depleted is 5 pF/pixel for the 73-channel device and 20 pF/pixel for the 19-channel diode.

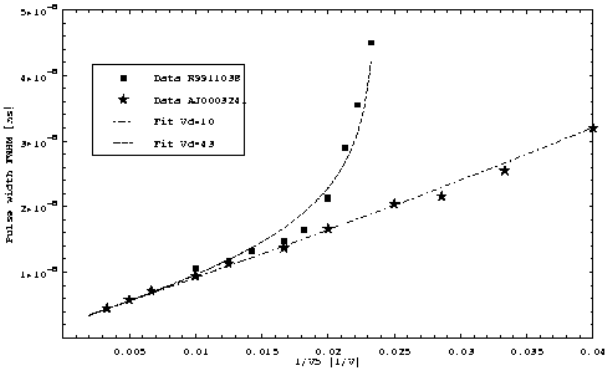

Fig. 3. Pulse width vs inverse bias voltage. Data (squares) from the earlier diodes fitted to the above model for pulse width shows that the width diverges quickly below the operating bias of 80 V, whereas the new diodes (stars) with lower depletion voltage have a 'linear' behavior as the voltage is decreased.

IV. Crosstalk

As work progressed on implementing the fast electronics required for the CMS readout, we discovered differential crosstalk between pixels that depended on the speed of the charge integration. This was not noticed when using the slower D0 preamplifiers and gated ADC's of the test beam. The 300 ohms/sq resistivity across the upper n+ layer and the 300 ohms resistance from back n+ bias contact to the front, provided insufficient current to respond to the faster pulses and shorter integration time, thus draining the neighboring pixels. The set of pulse shapes in Fig. 4 show the negative pulse induced in neighboring pixels by pixel 37 (the central illuminated pixel). Note that there is not much radial dependence in this differential crosstalk, so that even though it is only 1% per pixel, this adds up to 50 % over the whole tube. This is AC crosstalk, in that it only shows up for fast pulses and has its largest effect on tube performance in high rate experiments.

The AC crosstalk was reduced to <3% over the whole tube by applying a thin (25 nm) aluminum layer over the entire front surface. This reduced the resistivity to 1 ohms/sq. Conduction was extended to the back bias contacts via 100 nm thick aluminum traces at two edges of the diode. A SiO_2 barrier layer prevents diffusion of aluminum into n+ silicon.

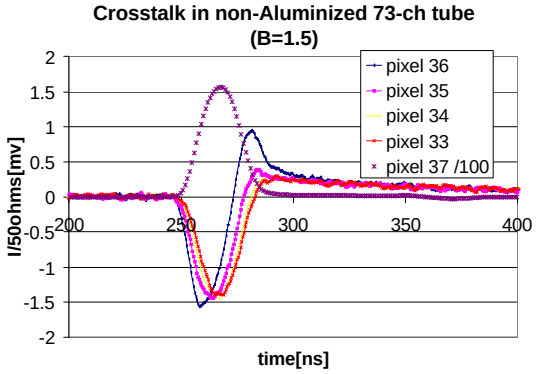

Fig. 4. AC crosstalk across a row of pixels. Light is injected into pixel 37.

A source of positive crosstalk now appears, which is due to backscattered electrons. The aluminization has actually made this contribution worse. By doing the same measurement in a magnetic field, we can eliminate the crosstalk due to backscatter by focussing it back into the same pixel. As can be seen from Fig. 5, this has improved the situation, but there is still a low level of positive crosstalk remaining. This turns out to be light which is not converted by the photocathode, reflecting off the front surface of the diode and having a second chance to produce photoelectrons when it again strikes the photocathode.

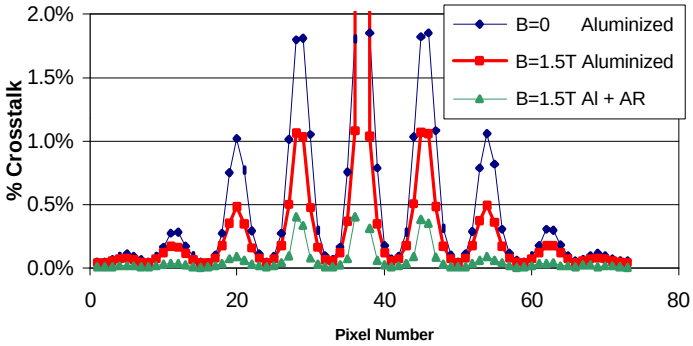

Fig. 5. The backscatter crosstalk across an entire aluminized 73-channel tube (B=0) compared to the remaining optical reflection crosstalk once the field is turned on. The lowest crosstalk is for the tube with an anti-reflective coating over the aluminized layer.

The radial dependence of the backscatter in an aluminized 19-channel tube was mapped by moving a 250 ìm fiber across one pixel and reading out the adjacent pixel. Thus, Fig. 6 represents the crosstalk experienced by one pixel as a function of where the input fiber is located on a neighboring pixel. The radial dependence is convoluted with the pixel shape, so the slope discontinuities represent moving beyond the hexagonal points of a pixel to larger area sampling.

Ballistic models in Fig. 7 show that the unconvoluted distribution is depleted close to the impact point, with more particles falling near a maximum radius which depends on the energy. The sharpness of the maximum is softened in the real case where a tail of lower energies also contribute. As the magnetic field is increased, the maximum range shortens and the central region becomes more populated, as paths begin to curl back to their origin. At higher magnetic field, minima occur in the particle range, corresponding to multiple windings before the particle returns to its origin, and causing the structure seen in the backscatter distributions with non-zero magnetic field of Fig. 7.

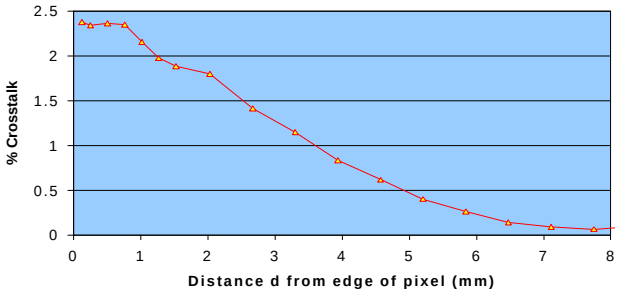

Fig. 6. Backscatter crosstalk (B=0) with optical crosstalk (B=1.5 T) subtracted for a bare silicon 19-channel HPD as a function of the position of the input light from the edge of the pixel read out. Crosstalk for fibers near the edge of the pixel compared to center.

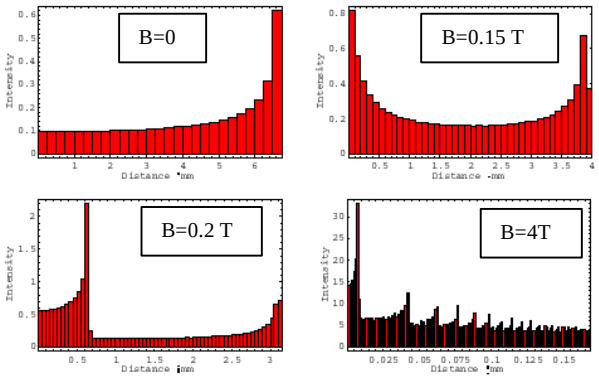

Fig. 7. Backscatter radial distributions: number of electrons as a function of distance from the impact point, for 10 keV electrons.

The fiber scan was also done for B=1.5 T, which therefore represents the optical reflection crosstalk. This was compared to a direct measurement of the reflected light off the internal diode using an avalanche photodiode on the surface of the HPD fiber optic faceplate, proving that optical reflection is responsible for the crosstalk which remains in the presence of a magnetic field. An interesting aside is that presumably all hybrid silicon devices have reflection crosstalk, since the reflectance of bare silicon at 40% is still significant, compared to 90% for our aluminum coating. This means that the true quantum efficiency of even a single channel HPD is less than the effective quantum efficiency, since the measured value always includes a second bounce.

V. Anti-reflective Coating

In order to eliminate crosstalk due to reflection, we studied how to apply an anti-reflective coating to the front surface of the aluminum. Our choices were guided by an optical modeling package for multilayer structures called IMD[6]. Our optimized formula called for 14 nm of hydrogenated amorphous silicon (a-Si:H) deposited over 25 nm of Al with a native layer of Al_2O_3 in between.

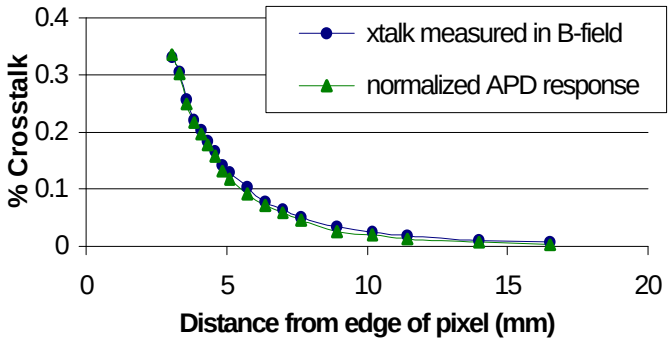

Fig. 8. Radial distribution of the optical reflection crosstalk: Circles represent the same procedure used for Fig. 6, but with B=1.5 T focusing the backscatter component away. Triangles are normalized measurements from direct detection of the light (using an avalanche photodiode) which makes it back through the photocathode due to reflection off the diode.

We made a series of test slides by plasma-enhanced chemical vapor deposition of a-Si:H (approximately 4% H by atomic weight) on glass slides with an initial 25 nm coating of aluminum, tuning the thickness (deposition time) of the silicon layer by comparing the wavelength minimum with the results from IMD. Reflectance as a function of wavelength and angle were measured by illuminating the slide with a monochrometer of 4 nm bandwidth and observing the reflected light with a PIN diode. The diode itself was also illuminated in the same position as the slide and its wavelength response divided out. The system properly observed a flat response from a 99% reflectivity mirror and from the bare aluminized slide. The wavelength of the monochrometer was checked with a calibrated filter. Our films matched the modeling program very well.

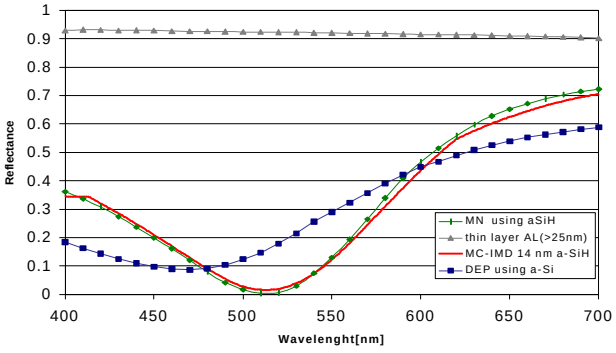

Fig. 9. 14 nm of a-Si:H deposited on aluminized glass slides matches the IMD optical modeling program. The bare aluminized slide has an approximately flat response at 92%. The DEP sputtered a-Si, with a minimum of 475 nm gives adequate reflection crosstalk reduction, but could be better optimized.

DEP then tried to apply the same coatings, using a sputtering technique and non-hydrogenous amorphous silicon. Our calculations predicted that they should use 16 nm of a-Si to achieve the same wavelength minimum as 14 nm of a-Si:H. We measured their samples in the same setup used for our slides. The DEP curve also shown in Fig. 9 can be reliably reproduced by DEP and provides adequate reduction in optical crosstalk at 520 nm.

Our success is measured in the crosstalk reduction finally obtained. The lowest curve in Fig. 5 shows that the crosstalk in a 73-channel aluminized tube with anti-reflective coating is only 0.4 % in the nearest neighbors when the B-field removes the backscatter component. It goes down to 0.1% at the next-nearest neighbors, which correspond to the nearest neighbors in the 19-channel tube. In summary: for the 73-channel tube, the total crosstalk in the whole tube (i.e. the amount of light removed from the illuminated pixel and spread about the tube) consists of 2 components:

	bare silicon	**Al coating**	**Al + a-Si:H**
(1) Backscatter	11%	13%	8%
(2) Optical reflection	7%	16%	4.3%

Total crosstalk in the 19-channel tube goes down by another factor of 4 for fibers at the center of the pixel and a factor of 2 for fibers near the edge of the pixel.

VI. Lifetime Issues

The tubes must be able to operate for 10 years in a radiation field (mostly MeV neutrons) reaching a maximum integrated dosage of 10^{11} n/cm². Integrated charge over that period can be as high as 3 C/pixel (off the anode) over a large bundle illuminating a 19-channel pixel at the most forward part of the barrel region [7]. Two 1 mm diameter WLS fibers are excited by blue light-emitting diodes (led's) and read out on one end by calibrated reference PIN diodes. The other end is potted into a cookie and retracted slightly from the HPD window such that the entire pixel is illuminated. The led's are set, one to deliver the maximum expected CMS charge in 10 months (middle graph) and the other to run at 1/10 the rate (top graph. The current from both reference diodes and the two HPD channels, as well as the temperature, are continuously monitored at time intervals of 30 minutes. Fig. 10 presents results from the most recent 73-channel aluminized tube (top trace) and for an earlier tube which encountered the high voltage problems mentioned in Section II (3). The current was tracked for about 23 weeks, normalized to reference diode and corrected for temperature. Since the maximum integrated charge on one 73-channel pixel was 1.8 C and its pixel area is a quarter of that of the larger pixels, this represents approximately 7 C on a 19-channel pixel. In all 4 of the tubes observed so far, there is an increase in the effective quantum efficiency for the first 100 mC of charge, after which the response falls off at less than 1% per CMS year.

Current spikes of greater than 100 nA will also trigger a reading in order to determine if internal sparking occurs, as shown in the bottom trace and in the lowest graph of Fig. 9, where the current off the high voltage supply is being monitored. The sparking design flaw has been corrected, but we still monitor all tubes in this way.

A duplicate of this station resides outside a retractable drawer of the University of Minnesota Cf^{252} irradiation facility. Quartz fibers link the led-stimulated WLS fibers to the HPD inside the MeV neutron field and continue to monitor the tube response in situ as exposure proceeds. Radiation damage produces an increase in leakage current proportional to the dose. The aluminized 73-channel tube behaved in the same way as earlier tubes [8], with the worst case scenario predicting a 5-10 nA/yr rise of leakage current for 19-channel pixels in the highest flux region.

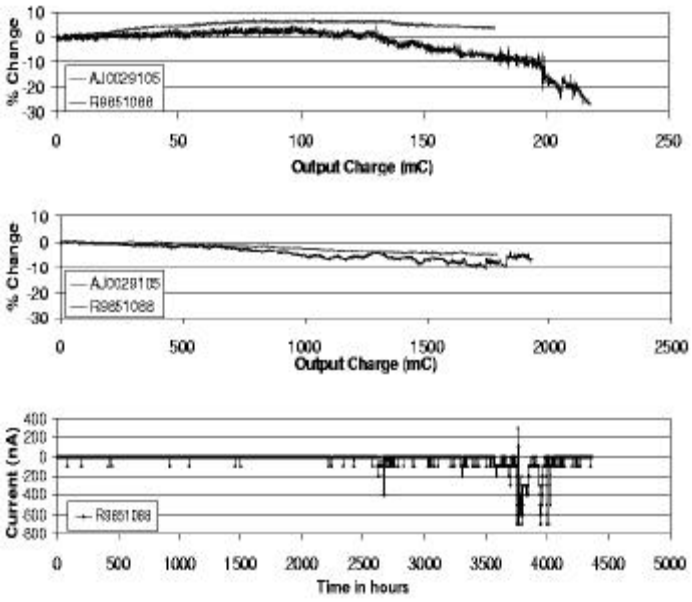

Fig. 10. Current as a function of total output charge off the anode, for 2 different pixels: top graph = CMS rate for 6 months, middle graph = Total of 6 CMS years in only 6 months. Aluminized 73-channel HPD lifetime curve is top trace; bottom trace is an early tube suffering sparking, which slowly destroys the internal vacuum. Bottom graph = high voltage supply current showing sparking problems in the early tubes.

VII. References

[1] CERN/LHCC 97-31, CMS TDR 2, 20 June 1997

[2] V. V. Abramov et al., "Studies of the response of the prototype CMS hadron calorimeter, including magnetic field effects, to pion, electron, and muon beams", Nucl. Instr. and Meth. A457 pp.75-100, 2001.

[3] P. Cushman, A. Heering, J. Nelson, C. Timmermans, S.R. Dugad, S. Katta, S. Tonwar, "Multi-pixel hybrid photodiode tubes for the CMS hadron calorimeter," Nucl. Instr. and Meth. A387, pp. 107-112, 1997.

[4] P. Cushman and R. Rusack, "A photomultiplier tube incorporating an avalanche photodiode", Nucl. Instr. and Meth. A333, pp381-390, 1993.

[5] P. Cushman, A. Heering, and A. Ronzhin, "Studies of hybrid photomultiplier tubes in magnetic fields up to 5 Tesla," Nucl. Instr. and Meth. A418, pp. 300-305, 1998.

[6] IMD Version 4.1.1, optical modeling package for multilayer structures by David L. Windt, http://cletus.phys.columbia.edu/windt/idl .

[7] P. Cushman, A. Heering, and A. Ronzhin, "Custom HPD readout for the CMS HCAL," Nucl. Instr. and Meth. A442, pp. 289-294, 2000.

[8] P. Cushman, A. Heering, and J.K. Nelson, "The effects of neutron irradiation on multi-pixel hybrid photodiode tubes," Nucl. Instr. and Meth. A411, pp. 304-312, 1998.